Two-step approach for pressure oscillations prediction in gas turbine combustion chambers

Dmytro Iurashev[1], Giovanni Campa[2], Vyacheslav V Anisimov[2] and Ezio Cosatto[2]

Abstract
Currently, gas turbine manufacturers frequently face the problem of strong acoustic combustion-driven oscillations inside combustion chambers. These combustion instabilities can cause extensive wear and sometimes even catastrophic damage of combustion hardware. This requires prevention of combustion instabilities, which, in turn, requires reliable and fast predictive tools. We have developed a two-step method to find a set of operating parameters under which gas turbines can be operated without going into self-excited pressure oscillations. As the first step, an unsteady Reynolds-averaged Navier–Stokes simulation with the flame speed closure model implemented in the OpenFOAM® environment is performed to obtain the flame transfer function of the combustion set-up. As the second step time-domain simulations employing low-order network model implemented in Simulink® are executed. In this work, we apply the proposed method to the Beschaufelter RingSpalt test rig developed at the Technische Universität München. The sensitivity of thermoacoustic stability to the length of a combustion chamber, flame position, gain and phase of flame transfer function and outlet reflection coefficient are studied.

1. Introduction
Nowadays gas turbine manufacturers have to meet ecological requirements, particularly, emissions of NO_X. These requirements force to produce gas turbines that work in lean combustion regime. However, the operation in lean combustion regime is characterised by the high probability of combustion instabilities occurrence (see the literature[1–3]), which may cause catastrophic damages. This requires prevention of combustion instabilities, which, in turn, requires the understanding of the nature of their occurrence.

There are different methods and numerical tools for prediction of combustion instabilities occurrence. The numerical tools used for thermoacoustic analysis could be divided into two groups: those that perform frequency domain analysis[4–6] and those that make time-domain simulations.[7,8] The first type of analysis can be applied to complex geometries of combustion chambers. The second type of tool for the prediction

of combustion instabilities occurrence consists in performing simulations in the time domain. However, brute force time-domain simulations of thermoacoustic processes in gas turbine chambers with complex geometries are extremely expensive from the computational point of view, especially, if there is a need to find the dependence of stability on different parameters of the system and a set of simulations has to be performed. This is the reason why we propose a method in which processes that happen on different scales are modelled in two different tools. This means that the analysis of turbulent reacting flow is conducted apart from the

[1]DICCA, Università degli studi di Genova, Genova, Italy
[2]Ansaldo Energia S.p.A., Genova, Italy

Corresponding author:
Dmytro Iurashev, DICCA, Università degli studi di Genova, Via Montallegro, 1, Genova 16145, Italy.
Email: dmytro.iurashev@edu.unige.it

acoustic analysis. Acoustic length- and time-scales are often considered to be much larger than chemical and turbulent scales. This makes possible to perform simulations of turbulent combustion and acoustics separately, using different tools. This decoupling is artificial but it helps to simplify the analysis.

First, the response of the flame to low-amplitude acoustic excitations is computed with the help of unsteady Reynolds-averaged Navier–Stokes (URANS) simulations using flame speed closure (FSC) model[9] implemented in OpenFOAM[10] environment. Compressible URANS simulations are employed because they yield reasonable precision for low-frequency excitations and are computationally cheaper than LES. It was reported that simulations with the FSC model give better agreement of heat release distributions with experimental data than simulations with the turbulent flame closure (TFC) model due to the improved treatment of the diffusion and the influence of the shear stress on the flame speed.[9] Thus, it is decided to use the FSC model in this approach. The set-up is excited with a broadband excitation and the unit impulse response (UIR) of heat release is calculated performing Wiener–Hopf inversion (WHI). Afterwards, the z-transform of the UIR is computed and as a result, the flame transfer function (FTF) of the set-up is obtained.

The analysis of linear waves is easier when the cross-section dimension of the combustor is small compared with the acoustic wavelength.[11] Then, acoustic modes with variations across the cross-sectional are 'cut-off', decaying with the axial position rather than propagating, and variations of the acoustic waves across the cross-section can be neglected. This leads to plane waves in a cylindrical combustor. The frequencies of interest for combustion instabilities in gas turbines are sufficiently low that this is often a good approximation. Then, the linear wave equations can be solved semi-analytically by a network approach.[12,13] This enables physical insight into important mechanisms. An acoustic network model implemented in Simulink is used as the second step of the proposed approach to find a set of parameters under which the set-up could be operated without going into self-excited pressure oscillations.

The FTF calculated at the first step is approximated with an analytical model and is used in the Simulink environment. In principle, distributed time-lag (DTL) model of the FTF proposed by Komarek and Polifke[14] can be used in the time-domain simulations in the network model. Rational time-lagged (RTL) transfer function model is able to give a better approximation of the calculated FTF and time-domain simulations with this model three orders of magnitude faster than with the DTL model. Thus, the RTL model is used in this work.

The approach presented in this work is developed primarily to calculate both the frequency and amplitude of combustion-driven pressure oscillations. It is possible to compute the latter, once the flame describing function (FDF) – the response of the flame to velocity perturbations of various amplitudes – is known. Linear stability of the set-up can also be predicted knowing just the FTF. There are a lot of works that perform thermoacoustic analysis in the frequency domain using network models. There are much fewer works that perform time-domain simulations. Some of them are concentrated on simple thermoacoustic systems such as Rijke tube,[8,15] some are applied to more complicated laboratory set-ups[16–18] and some to industrial test rigs.[19] This work applies time-domain analysis with a network model to the complex combustion system. Linear analysis is performed in this work.

In the current work, the proposed two-step method is tested on the Beschaufelter RingSpalt (BRS) test rig developed by Komarek and Polifke[14] at the Technische Universität München. Dependence of stable and unstable frequencies of the set-up on the combustion chamber length, the position of the flame, the gain and phase of the FTF and the outlet reflection coefficient is discussed.

2. Background

2.1. Description of the FSC model

In order to model the combustion in the BRS test rig, we use FSC model proposed by Lipatnikov and Chomiak.[9] We have implemented this flame model into the environment of OpenFOAM.[20] The compressible PIMPLE (merged PISO-SIMPLE) algorithm is used. The FSC model makes use of the regress variable, i.e. the normalised fuel mass fraction, defined as

$$b = \frac{T_b - T}{T_b - T_u} \tag{1}$$

where T_b is the temperature of the burnt gas, T is the temperature of the gas at the current point and T_u is the temperature of the unburnt gas. Thus, regress variable is equal to 1 in the zone of unburnt gas and to 0 in the zone of burnt gas.

In contrary to TFC model,[21] the FSC model describes the propagation of the flame in the limit case of the absence of turbulence as well as in the case of fully developed turbulence. Moreover, it takes into account the dependence of turbulent diffusivity and turbulent flame speed on the time of flow propagation from the flame holder to the flame front.

The transport equation for the regress variable is

$$\frac{\partial \rho b}{\partial t} + \nabla \cdot (\rho \mathbf{U} b) - \nabla \cdot \left[\rho(\kappa + D_{t,t})\nabla b \right]$$
$$= -\frac{S_{L,0}^2}{4(\kappa + D_{t,t})} \rho_u (1-b)b - \rho_u S_{t,t} |\nabla b| \tag{2}$$

where ρ is the density of the air–fuel mixture, t is the time, $\mathbf{U}$ is the vector of the mean velocity, κ is the molecular diffusivity, $D_{t,t}$ is the time-dependent coefficient of turbulent diffusion, $S_{L,0}$ is the unperturbed laminar flame speed and $S_{t,t}$ is the time-dependent turbulent flame velocity. The time-dependent coefficient of turbulent diffusion is calculated as

$$D_{t,t} = D_t \left[1 - \exp\left(-\frac{t_{fd}}{t_L} \right) \right] \tag{3}$$

where D_t is the coefficient of turbulent diffusion, t_{fd} is the flame development time, t_L is the Lagrangian time scale of turbulence, calculated as $t_L = D_t/u'^2$, where u' is the velocity perturbation. The coefficient of turbulent diffusion is calculated as $D_t = \mu_t/(\rho Sc_t)$, where μ_t is the turbulent viscosity and Sc_t is the turbulent Schmidt number. The flame development time is calculated as follows

$$t_{fd} = \frac{x - x_{fh}}{u_{FSC}} \tag{4}$$

where x is the current axial position, x_{fh} is the axial position of the flame holder and u_{FSC} is the axial flow velocity at the burner exit. The turbulent flame velocity which depends on the flame development time is calculated as

$$S_{t,t} = S_t \left\{ 1 + \frac{t_L}{t_{fd}} \left[\exp\left(-\frac{t_{fd}}{t_L} \right) - 1 \right] \right\}^{0.5} \tag{5}$$

where S_t is the turbulent flame speed, calculated as

$$S_t = A(u')^{0.75} S_{L,0}^{0.5} \alpha_u^{-0.25} l_t^{0.25} \tag{6}$$

where A is the model dimensionless constant taken to be equal to 0.52, as recommended by authors of the FSC model[9]; α_u is the thermal diffusivity of the unburnt mixture and l_t is the turbulence length scale that is calculated as

$$l_t = C_D \frac{(u')^3}{\epsilon} \tag{7}$$

where C_D is the model dimensionless constant and ϵ is the turbulence dissipation rate. The heat release rate is

proportional to the RHS of equation (2), i.e.

$$\dot{Q} \propto \frac{S_{L,0}^2}{4(\kappa + D_{t,t})} \rho_u (1-b)b + \rho_u S_{t,t} |\nabla b| \tag{8}$$

2.2. FTF

The dynamic response of a flame to a flow perturbation of small amplitudes can be represented in the frequency domain by its $FTF(\omega)$ (also called frequency response of the flame). It relates fluctuations of the flame heat release $\dot{Q}'$ to fluctuations of velocity u_r' at a reference position r upstream of the flame

$$FTF(\omega) = \frac{\hat{\dot{Q}}(\omega)/\bar{\dot{Q}}}{\hat{u}_r(\omega)/\bar{u}_r} \tag{9}$$

Here fast Fourier transforms $\hat{\dot{Q}}$ and $\hat{u}_r$ of fluctuations $\dot{Q}'$ and u_r' are normalised against the respective mean values of heat release $\bar{\dot{Q}}$ and velocity $\bar{u}_r$. In experiments $FTF(\omega)$ was computed from time series of fluctuations u_r' and $\dot{Q}'$ with spectral analysis applying harmonic excitation with a loudspeaker at the inlet. In numerical simulations, the advanced method based on WHI can be used.

2.3. WHI

Application of the WHI to results of unsteady CFD simulations in order to find the FTF of a burner was initially proposed by Polifke et al.[22] This method reconstructs the UIR of the flame to the velocity perturbation and then transforms it into the frequency response using the z-transform

$$FTF(\omega) = \sum_{k=0}^{L} h_k e^{-i\omega k \Delta t} \tag{10}$$

where Δt is the time step for the time series data record, h_k are coefficients of the UIR; to find them, the auto-correlation matrix Γ and the cross-correlation vector $\mathbf{c}$ of the time series data $(u_k', \dot{Q}_k')$ for $k = 0, \dots, N$ are calculated as follows

$$\Gamma_{ij} = \frac{1}{N - L + 1} \sum_{k=L}^{N} \frac{u_{k-i}'}{\bar{u}} \frac{u_{k-j}'}{\bar{u}} \quad \text{for} \quad i, j = 0, \dots, L \tag{11}$$

$$c_i = \frac{1}{N - L + 1} \sum_{k=L}^{N} \frac{u_{k-i}'}{\bar{u}} \frac{\dot{Q}_k'}{\bar{\dot{Q}}} \quad \text{for} \quad i = 0, \dots, L \tag{12}$$
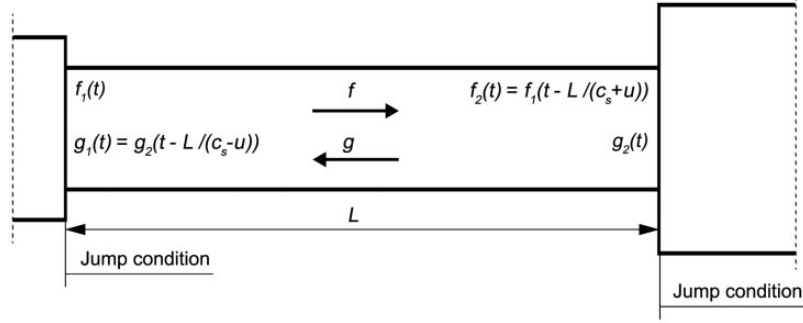
Figure 1. Scheme of waves propagation in a section of a low-order model.

where N is the number of points in the vector of the signal time series, L is the assumed length of the vector of the UIR, the filter 'memory'. To find the vector of coefficients of the UIR, the WHI is performed

$$\mathbf{h} = \Gamma^{-1}\mathbf{c} \qquad (13)$$

This method allows computing FTF in the wide range of frequencies performing just one run. As a result, it is a fast method for FTF calculation.

2.4. Wave-based approach for thermoacoustic simulations

The length of the test rig considered in this work is much larger than its dimensions in the other directions. Thus, it is possible to perform a one-dimensional low-order acoustic analysis.

The test rig is divided into a set of sections with constant cross-sectional area. Pressure, velocity, temperature and density are decomposed into the sum of their mean component (denoted by ⁻) and their fluctuating component (denoted by ′). Mean values of pressure, velocity, temperature, density and thermophysical properties are assumed to be constant along each section and are changing only from section to section.

Perturbations of pressure and velocity could be represented in terms of downstream and upstream propagating acoustic waves (characteristics) (see Figure 1)

$$p'(x, t) = f\left(t - \frac{x}{\bar{c}_s + \bar{u}}\right) + g\left(t + \frac{x}{\bar{c}_s - \bar{u}}\right) \qquad (14)$$

$$u'(x, t) = \frac{1}{\bar{\rho}\bar{c}_s}\left[f\left(t - \frac{x}{\bar{c}_s + \bar{u}}\right) - g\left(t + \frac{x}{\bar{c}_s - \bar{u}}\right)\right] \qquad (15)$$

$$\rho'(x, t) = \frac{1}{\bar{c}_s^2}\left[f\left(t - \frac{x}{\bar{c}_s + \bar{u}}\right) + g\left(t + \frac{x}{\bar{c}_s - \bar{u}}\right)\right] \qquad (16)$$
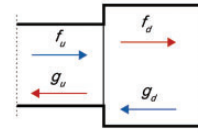

Figure 2. Scheme of waves propagation between sections of a low-order model.

where p' is the fluctuating pressure; f and g are downstream and upstream travelling components of acoustic waves, respectively; $\bar{c}_s$ is the mean speed of sound; $\bar{u}$ is the mean velocity; u' is the fluctuating velocity; $\bar{\rho}$ is the mean density and ρ' is the fluctuating density.

In order to connect oscillating variables in different sections (see Figure 2), we need to know the so-called jump conditions. Jump conditions between sections with different cross-section area are calculated by solving the system of linearised equations of conservation of mass and energy (Bernoulli) in terms of f and g as suggested by Dowling and Stow.[11] We can write the system of equations in case of area change in matrix form as follows

$$\mathbf{F}\begin{bmatrix} f_d \\ g_u \end{bmatrix} = \mathbf{K}\begin{bmatrix} f_u \\ g_d \end{bmatrix} \qquad (17)$$

where subscripts u and d denote upstream and downstream sections, respectively. The coefficients of matrices $\mathbf{F}$ and $\mathbf{K}$ can be found in Appendix 1.

To calculate jump conditions at the flame, the system of linearised equations of conservation of momentum and energy has to be solved in terms of f and g. The system of equations in matrix form at the flame is

$$\mathbf{J}\begin{bmatrix} f_d \\ g_u \end{bmatrix} = \mathbf{H}\begin{bmatrix} f_u \\ g_d \\ \dot{Q}' \end{bmatrix} \qquad (18)$$

where coefficients of matrices **J** and **H** can be found in Appendix 1.

At the beginning of the first section and at the end of the last section f and g waves are related by the reflection coefficients R_{in} and R_{out}, respectively.

3. Step 1. Modelling the FTF

3.1. Description of the experimental set-up

The test rig under consideration is operated under atmospheric pressure and consists of three main parts: a plenum, a swirl stabilised burner with a central bluff body and a combustion chamber (see Figure 3). A perfectly premixed mixture of methane and air with equivalence ratio equal to 0.77 enters in the set-up. The plenum is a cylinder with the diameter of 200 mm and length of 170 mm. A rigid sinter metal plate is placed at the beginning of the plenum. The burner exit is represented by an annular section with an inner diameter of 16 mm and an outer diameter of 40 mm. The swirler consists of eight blades with the length of 30 mm is positioned 30 mm upstream the burner exit. The length of the burner duct is 180 mm. The combustion chamber has the quadratic cross-section of 90×90 mm^2. The length of the combustion chamber is variable and during FTF measurements was kept equal to 300 mm. A perforated plate was placed at the end of the combustion chamber in order to ensure a low reflective acoustic boundary condition. Walls of the experimental set-up were made of glass in order to be able to observe the flame and are water cooled. In the experiments, the position of the heat release distribution was determined by OH* chemiluminescence measurements. Further details about experimental set-up can be found in the work of Komarek and Polifke.[14]

The set-up under consideration is perfectly premixed; thus the heat release is sensitive only to velocity perturbations and equation (9) can be used to describe the flame dynamics. In the experiments, the velocity was perturbed at the inlet of the plenum and the velocity perturbations for the FTF calculation were measured in experiments 7 cm upstream of the burner exit
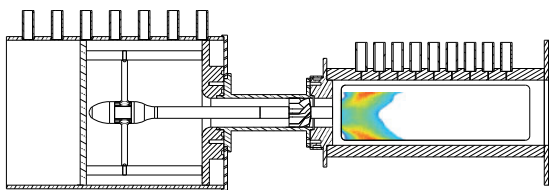
(1 cm upstream of the swirler).[23] The position upstream the swirler is chosen to avoid strong turbulent fluctuations produced by the swirler.[24]

3.2. Description of the numerical set-up

Since the main goal of the simulations is to calculate the flame dynamics, the effect of the plenum on the fluid dynamics in the chamber is assumed to be negligible and the plenum is not considered in the numerical set-up. The length of the burner duct in the simulations is reduced to 160 mm. For simulations, the combustor length of 200 mm is used for the sake of computational costs. The heat release zone lies in the first 100 mm of the combustion chamber, as reported by Komarek and Polifke.[14] It will be shown in the next section that the recirculation zone lies within the computational domain. Thus, it is shown a posteriori that the considered combustor length is enough to simulate the behaviour of the flame. Since the structure of the set-up is periodical, just one-quarter of the test rig has been modelled in the simulations (see Figure 4). A 3D structured mesh consisting of around 280,000 cells is created using the commercial software ANSYS® ICEM CFD^{TM}. The time step of the simulations is 4×10^{-7} s to ensure an acoustic CFL number lower than 0.7.

In the investigation, the thermal power is equal to 30 kW. To avoid the development of resonance modes in perturbed simulations, partially reflective boundary conditions at the inlet and at the outlet have been employed. The *wave transmissive* boundary condition of OpenFOAM[10] is used in this work. This condition is based on the work of Poinsot and Lele[25] and is expressed as

$$\frac{\partial p}{\partial t} + u_{wave} \frac{\partial p}{\partial x} = \frac{u_{wave}}{l_{inf}}(p_{inf} - p) \qquad (19)$$

where $u_{wave} = u + c_s$ at the outlet, $u_{wave} = u - c_s$ at the inlet, c_s is the speed of sound, l_{inf} is the distance from the boundary (outlet or inlet) at which the pressure field p
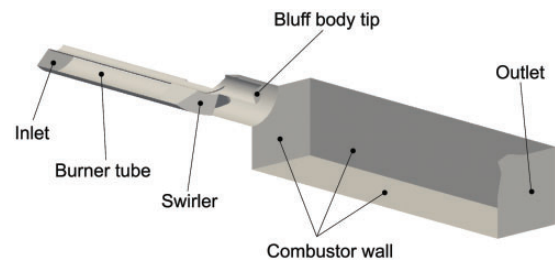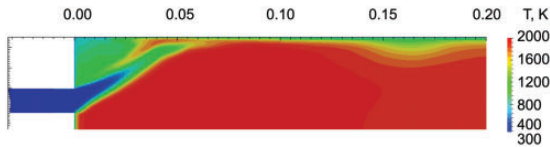

Figure 3. Scheme of the experimental set-up of the BRS test rig (image courtesy of Thomas Komarek). BRS: Beschaufelter RingSpalt.

Figure 4. Sector scheme of the CFD computational domain of the BRS test rig. BRS: Beschaufelter RingSpalt; CFD: Computational Fluid Dynamics.

Table 1. Boundary conditions for the BRS numerical model.

Face	Boundary condition	Details
Inlet	Velocity inlet	11.3 m/s
Outlet	Pressure outlet	101,325 Pa
Burner tube, swirler	Adiabatic no-slip wall	–
Combustor wall	Isothermal no-slip wall	600 K
Bluff body tip	Isothermal no-slip wall	600 K

BRS: Beschaufelter RingSpalt.

Figure 5. Temperature distribution in the longitudinal cross-plane; unperturbed simulation.

Figure 6. OH* chemiluminescence distribution from experiment[23] and heat release distribution from simulation along the longitudinal axis.

Figure 7. Velocity excitation used in the FTF calculation. FTF: flame transfer function.

becomes 0; in this work, $l_{inf} = 1$ m. Boundary conditions for the unperturbed simulation are listed in Table 1.
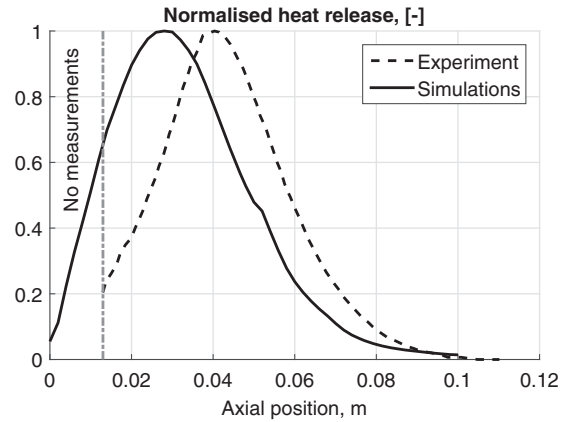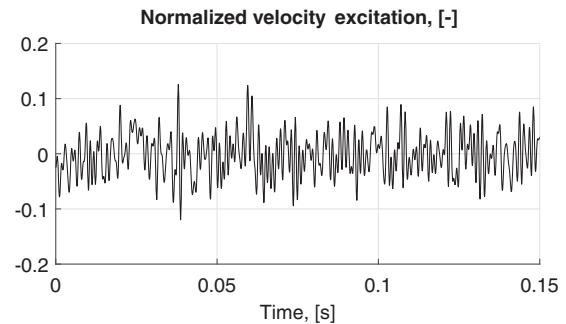
Walls of the experimental set-up under consideration are made of glass in order to be able to observe the flame and they are water cooled. The temperature of the combustor walls is imposed to 600 K to take into account heat losses, as suggested by Tay-Wo-Chong et al.[23]

3.3. Results of unperturbed simulations

In a previous work of ours (see Iurashev et al.[20]) a sensitivity analysis of the parameters of the FSC model was performed. As a result, the following values of parameters were chosen: the turbulent Schmidt number $Sc_t = 0.3$, the model constant $C_D = 0.3$ and the axial flow velocity at the burner exit $u_{FSC} = 18$ m/s. The last value is larger than inlet velocity because of the funnelling effect of the jet. Field of temperature in the longitudinal cross-section obtained from unperturbed simulation is shown in Figure 5.

It is illustrative to compare the distributions of heat release in experiments and simulations along the longitudinal axis. To obtain this distribution from our simulation we take several planes perpendicular to the longitudinal axis in the range $0 - 0.1$ m from the beginning of the combustion chamber in the axial direction. Then, we calculate area-averaged values of the heat release over these planes and plot the resulting values over the longitudinal axis (see Figure 6).

The difference between experimental and numerical heat release distributions is explained by the presence of the flame both in the inner and outer shear layers in simulation (so-called M-flame). However, in the experiments the flame was observed mostly in the inner shear

layer, that is called V-flame. This is explained by the fact that the FSC model was developed for adiabatic cases, meanwhile, the experimental set-up is non-adiabatic.

3.4. FTF numerical calculation

A transient numerical simulation of the system is performed exciting the velocity at the inlet of the computational domain. The signal of excitation is composed of a sum of sine waves with random frequencies in the range 0–1 kHz and random phase. The excitation signal is normalised in a way that three standard deviations of the signal amplitude are equal to 10% of the mean velocity at the inlet to the computational domain; it is shown in Figure 7. The fast Fourier transform of the velocity excitation signal is shown in Figure 8. The excitation signal is added to the mean velocity at the inlet denoted in Table 1.

The time series u_r is composed during the simulations as the axial component of velocity averaged in the plane perpendicular to the z-axis situated 2 cm upstream of the burner exit (1 cm downstream of the swirler). The reference plane for the velocity
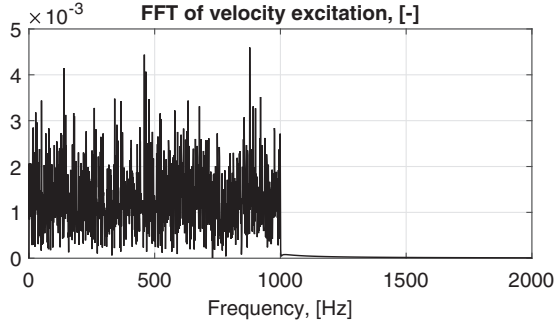
Figure 8. Fast Fourier transform of the velocity excitation imposed at the inlet of the computational domain.
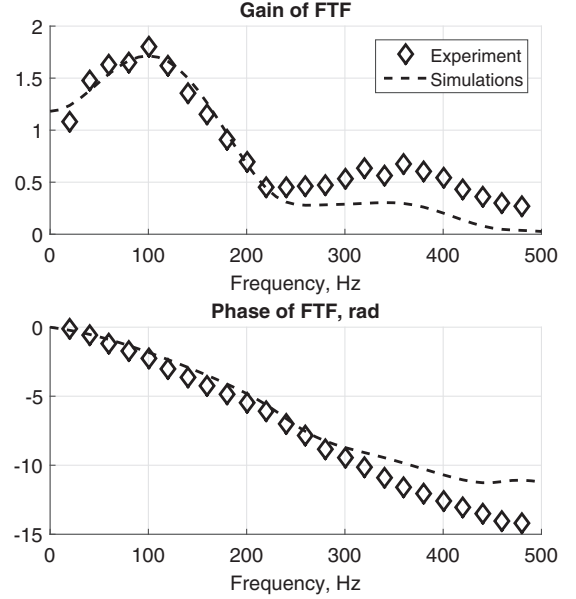

Figure 9. FTF of the BRS test rig obtained experimentally and from OpenFOAM simulations. BRS: Beschaufelter RingSpalt; FTF: flame transfer function.

perturbation measurement differs from the experimental position. As noted by Tay-Wo-Chong Hilares,[24] there is no significant impact on the calculated FTF if the velocity perturbations are measured in the range $0 - 7$ cm upstream the burner exit. The response of the flame $\dot{Q}$ is computed in simulations as the volumetric integral of equation (8). After that, the mean values $\bar{u}_r$ and $\bar{\dot{Q}}$ of calculated u_r and $\dot{Q}$ are computed and are subtracted from series of u_r and $\dot{Q}$, respectively, in order to obtain fluctuations of the axial velocity u'_r and fluctuations of the heat release $\dot{Q}'$.

The simulation is run for 129 ms in real time. Longer simulation times do not change the FTF. The duration of the UIR is assumed to be $L\Delta t = 10$ ms, where $\Delta t = 4 \times 10^{-5}$ s. The first 15 ms are considered as a transition period and are neglected. Using the WHI method described before, the FTF of the BRS test rig is calculated. The results are shown in Figure 9.

There is a good agreement between the experimentally obtained FTF and the one obtained with simulations in terms of gain of the FTF in the range of frequencies from 0 till 300 Hz. The shift in phase of the FTF is explained by the shifted distribution of the heat release from simulations with respect to the experimental one shown in Figure 6.

4. Step 2. Stability analysis using wave-based approach

4.1. Low-order network model set-up

The numerical set-up that represents BRS test rig has been divided into six regions with three jump conditions with pressure losses, one jump condition at the flame and two boundary conditions as shown in Figure 10. The cross-sectional area, length and temperature of each section are listed in Table 2. Jump matrices to connect waves between sections are calculated using systems of equations (17) and (18). The reflection coefficient of the plenum inlet is taken $R_{in} = 1$. The outlet
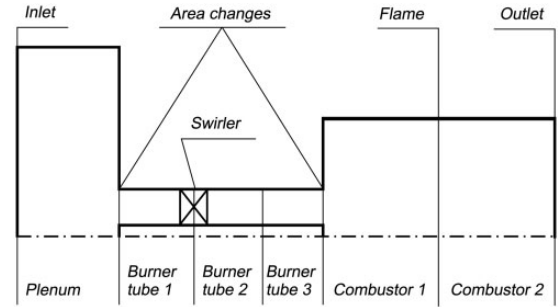
Figure 10. Scheme of network model numerical set-up divided into sections.

Table 2. Values of parameters imposed in the network model.

N	Section	Area (m²)	Length (m)	Temperature (K)
1	Plenum	$3.146E-2$	0.17	300
2	Burner tube 1	$1.056E-3$	0.135	300
3	Burner tube 2	$1.056E-3$	0.025	300
4	Burner tube 3	$1.056E-3$	0.02	300
5	Combustor 1	$8.1E-3$	x_{flame}	300
6	Combustor 2	$8.1E-3$	$L_{c.c.} - x_{flame}$	1930

reflection coefficient $R_{out} = -0.4$ approximated from the values suggested by Tay-Wo-Chong et al.[23] is used unless another value is specified. The total length of the combustor (sum of the lengths of *Combustor 1* and *Combustor 2*) is $L_{c.c.} = 0.7$ m unless another value

is specified. Acoustic losses at area changes between the plenum and the burner tube and between the burner tube and the combustor are taken into account by coefficients of pressure losses $\zeta_{decr} = 0.487$ and $\zeta_{incr} = 0.756$, respectively, calculated by formulae proposed by Idelchik.[26] Acoustic losses at the swirler are taken into account by the coefficient of pressure losses $\zeta_{swirler} = 2.073$ calculated from the unperturbed OpenFOAM simulations. The active flame, i.e. the unsteady heat release, in low-order network model is positioned at $x_{flame} = 0.03$ m unless another value is specified. This value corresponds to the maximum of the heat release in the longitudinal direction in OpenFOAM simulations (see Figure 6). The temperature in the last network model section in this work is equal to 1930 K that is identical to the one in the work of Tay-Wo-Chong et al.[23] in order to compare the results. This value is close to the adiabatic temperature of the flame (1960 K) that is observed in the inner recirculation zone in the OpenFOAM simulations (see Figure 5). The temperature gradient at the flame in the network model is important for the stability prediction.[27]

The velocity fluctuations for the unsteady heat release model are taken between sections *Burner tube 2* and *Burner tube 3* that correspond to the velocity probe position in the simulations.

The set-up is excited at the inlet for the first $t_{exc} = 0.1$ s of simulations by the signal composed of sine functions with the frequency in the range $0 - 1$ kHz with the maximum amplitude 5 Pa. After 0.1 s till 1.0 s of simulations, the system is left to evolve by itself without external excitation. The parameter called growth rate is used; it gives information if the mode is stable or not. It is possible to calculate the growth rate from the time-domain simulations assuming the following law for the pressure perturbations

$$p'(t) = \sum_{i=1}^{n} P_i \sin(2\pi f_i t + \phi_i) e^{\alpha_i(t - t_{exc})} \quad (20)$$

where f_i is one of the frequencies of pressure oscillations after t_{exc}, n is the number of the frequencies of pressure oscillations after t_{exc}, P_i is the amplitude of pressure oscillations at f_i at the time t_{exc}, ϕ_i is the phase of the pressure oscillations at f_i and α_i is the growth rate of the mode f_i.

The frequencies of oscillations and their growth rates are computed by approximating time history of pressure oscillations by equation (20) using the least-squares method. In the simulations presented in this work, either one or none unstable frequency per run is detected, thus $n = 1$ for all simulations in the network model. Positive values of growth rate parameter α

indicate that the system is unstable, and the negative values of α mean that the system is stable.

4.2. FTF approximation for the network model

The FTF obtained from OpenFOAM simulations is inserted in the network model environment in the RTL form

$$FTF_{model}(\omega) = \left[\frac{n_{f,1}\omega_{0,1}^2}{-\omega^2 + 2i\xi_1\omega_{0,1}\omega + \omega_{0,1}^2} + \right. \quad (21)$$

$$\left. \sum_{j=2}^{3} \frac{2in_{f,j}\xi_j\omega_{0,j}\omega}{-\omega^2 + 2i\xi_j\omega_{0,j}\omega + \omega_{0,j}^2} + \right] e^{-i\omega\tau_f} \quad (22)$$

where $n_{f,i}$ is the dimensionless constant, $\omega_{0,1}$ is the cut-off frequency of the second-order low-pass filter, ξ_i is the damping ratio, $\omega_{0,2}$ and $\omega_{0,3}$ are band-pass frequencies and τ_f is the time delay of the flame. Optimum values of coefficients of equation (22) are computed using the least-squares method.

Values of the model coefficients of the FTF calculated with URANS simulations are listed in Table 3; time delay for the flame model is $\tau_f = 1.163 \cdot 10^{-3}$ s. The resulting FTF model is shown in Figure 11 together with the FTF obtained from simulations.

4.3. Results of network model simulations

An unstable frequency at 101.3 Hz was detected in experiments with a combustor length of 0.7 m as noted by Tay-Wo-Chong and Polifke.[28] With the length of combustor equal to 0.3 m, the set-up was stable.[28]

It is worth to mention that this unstable frequency is denoted by Bomberg et al.[29] as 'flame-intrinsic' mode and by Silva et al.[27] as 'intrinsic thermoacoustic' (ITA) mode. The brief explanation of the ITA mode formation is given in Figure 12. The heat release perturbations $\dot{Q}'$ according to equation (18) produce acoustic waves and one of them, g_5, travels upstream to the junction between the combustor and the burner tube. At this junction, according to equation (17), one part of the acoustic wave g_5 transforms into the wave g_4 that

Table 3. Coefficients of the model of the FTF computed with simulations.

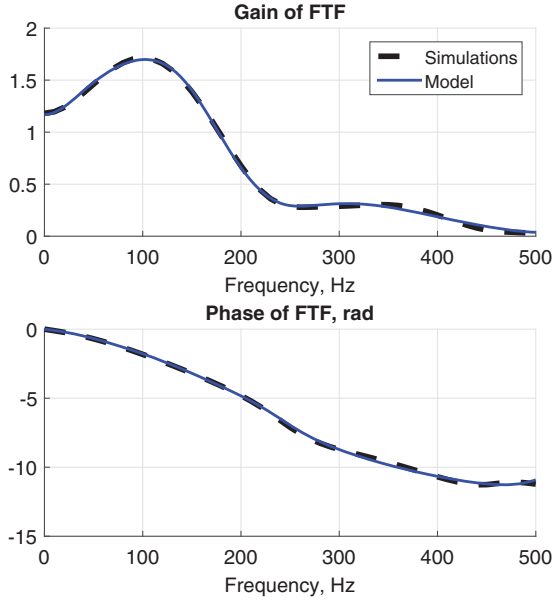| j	n_{fj}	ω_{0j}	ξ_j
1	1.169	2160	0.461
2	1.156	1267	1.612
3	−3.232	1073	0.455

FTF: flame transfer function.

Figure 11. FTF of the BRS test rig from OpenFOAM simulations and modelled with equation (22). BRS: Beschaufelter RingSpalt; FTF: flame transfer function.
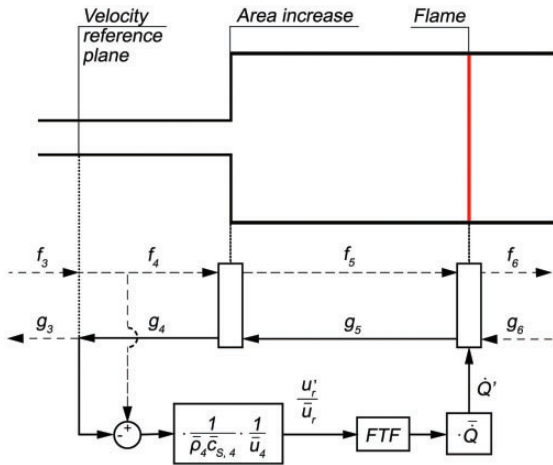

Figure 12. Scheme of formation of ITA modes. ITA: intrinsic thermoacoustic.

Figure 13. Acoustic response of the flame.

The acoustic response of the flame defined by Bomberg et al.[29] as $S_{21} = \frac{g_4}{f_4}$ is calculated by performing simulations in the network model considering only sections *Burner tube 3* and *Combustor 1*, as shown in Figure 12. The dependence of S_{21} on the frequency is computed using WHI described above using f_4 and g_4 instead of $\frac{u'_k}{\bar{u}}$ and $\frac{\dot{Q}'_k}{\bar{\dot{Q}}}$, respectively. The resulting $S_{21}(\omega)$ is shown in Figure 13. The maximum value of S_{21} corresponds to the frequency 143 Hz.

According to calculations of Bomberg et al.,[29] this mode by itself is stable but pressure oscillations were observed at this frequency in experiments.[23] This is because Bomberg et al.[29] considered only the system that consists of the burner tube, the area increase, the combustion chamber and the unsteady heat release. Reflection coefficients both at the inlet of the burner tube and at the outlet of the combustor were taken equal to 0, i.e. no waves reflected from the burner inlet or combustor outlet were considered. Once the plenum is added into consideration, the stability of the ITA mode changes. The effect of adding the plenum with a cross-section area much larger than the burner tube cross-section area is similar to a negative inlet reflection coefficient. And it was shown by Silva et al.[27] that decrease of the inlet reflection coefficient makes the ITA mode more unstable. Thus, the plenum existence is one of the factors responsible for the instability of the ITA mode in the BRS set-up.

Sensitivity to combustor length. A parametric study with different values of the combustion chamber length in the range $0.3 - 1.1$ m with steps of 0.1 m is performed. For values of the combustion chamber length below and equal to 0.6 m the set-up is stable (see Figure 14). For combustion chamber lengths equal or higher than 0.7 m, the set-up is unstable. Thus, our simulations predict the set-up with the length of combustion chamber $L_{c.c.} = 0.3$ m to be stable and with $L_{c.c.} = 0.7$ m to be unstable as in the experiments. The unstable frequency calculated for $L_{c.c.} = 0.7 - 1.1$ m is around $130 - 135$ Hz and does not depend significantly on the

travels to the reference velocity plane. At this plane, the acoustic wave g_4 contributes to the velocity perturbations u'_r that produce heat release oscillations through the FTF. At this point, the loop is closed; since this loop can exist even with the zero reflection coefficients,[27] the acoustic mode produced as a result of this interaction is called intrinsic. Nevertheless, it does not imply that acoustics of the set-up does not influence the frequency and the stability of the intrinsic mode. The more detailed explanation of the ITA mode formation can be found in the work of Bomberg et al.[29]
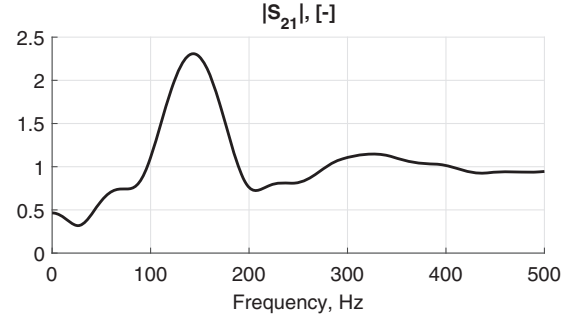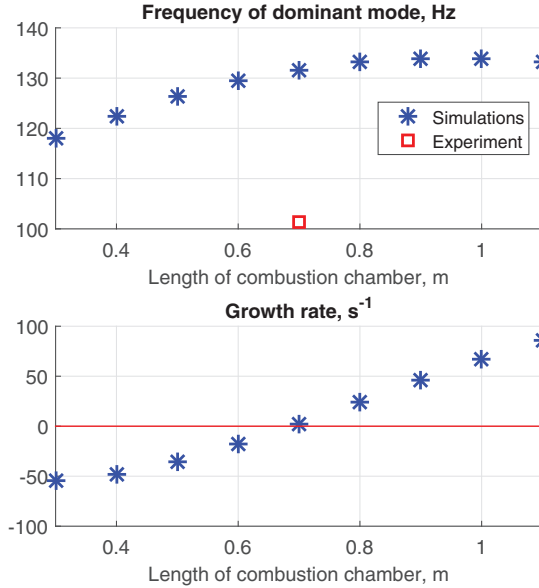
Figure 14. Dominant frequency of oscillations and its growth rate for various length of combustion chamber; $x_{flame} = 0.03$ m, $k_G = 1$, $\tau_{add} = 0$ ms.

Figure 15. Dominant frequency of oscillations and its growth rate for various positions of unsteady heat release; $L_{c.c} = 0.7$ m, $k_G = 1$, $\tau_{add} = 0$ ms.

total length of the combustion chamber. The computed frequencies are significantly higher than the one retrieved in experiments. The computed frequencies are close to the frequency of the maximum of S_{21} shown in Figure 13. The difference is explained by the influence of the acoustics of the system on the ITA mode.

The FSC model that is used in this work is adiabatic as well as the TFC model used by Tay-Wo-Chong et al.[23] However, using the FTF computed with the URANS simulations and the TFC model predicted the BRS test rig to be unstable only with the total combustor length equal or higher than 1 m. The unstable frequency obtained by Tay-Wo-Chong et al.[23] is also higher than the one detected in experiments. It is mentioned by Tay-Wo-Chong et al.[23] that three parameters were different for the experimental measurements and the URANS simulations with the TFC model: the position of the maximum heat release of the unperturbed case (denoted here as x_{flame}), the gain and the phase of the FTF around the unstable frequency. To investigate these aspects, we perform a parametric analysis varying the position of the unsteady heat release, the gain and the phase of the FTF in the network model. We are aware of the strong connection between the heat release distribution and the phase of FTF. First, the direct effect of heat release distribution, i.e. the flame position in the network model, and its indirect effect, i.e. the phase of the FTF, on the stability are studied separately in this work to understand the effect of each component. Then, the combined effect of the simultaneous change of the flame position and the FTF phase on the thermoacoustic stability is studied.
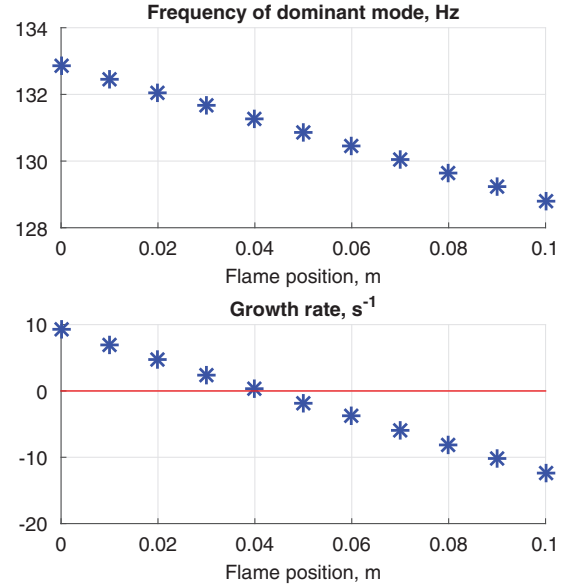
Sensitivity to the flame length. We vary the parameter x_{flame} in the range $0 - 0.1$ m with steps of 0.01 m keeping fixed length of the combustion chamber $L_{c.c} = 0.7$ m and the fixed FTF. This range corresponds to the heat release distribution in the longitudinal direction (see Figure 6). As it can be seen from Figure 15, the thermoacoustic system is unstable for values of the x_{flame} smaller or equal to 0.04 m. When increasing the x_{flame} parameter, the frequency of the dominant mode of the set-up slightly decreases. The dependence of the growth rate of this mode α_{dom} on the position of the flame is not as steep as for the dependence of α_{dom} on the length of the combustion chamber.

To study the influence of the gain and the phase of the FTF on the stability of the set-up, we introduce the modified version of the model for the FTF

$$FTF_{model,2}(\omega) = k_G FTF_{model}(\omega)e^{-i\omega\tau_{add}} \qquad (23)$$

where k_G is the dimensionless parameter responsible for the change of the gain of the FTF and τ_{add} is the additional time delay responsible for the change of the phase of the FTF.

Sensitivity to the gain of FTF. Next, we change the parameter k_G in the range $0.8 - 1.2$ with steps of 0.05. It is seen from Figure 16 that the set-up is stable for values of k_G lower than 1, i.e. lower values of the gain of the FTF. The dominant frequency of the oscillations of the set-up is slowly growing when k_G increases.
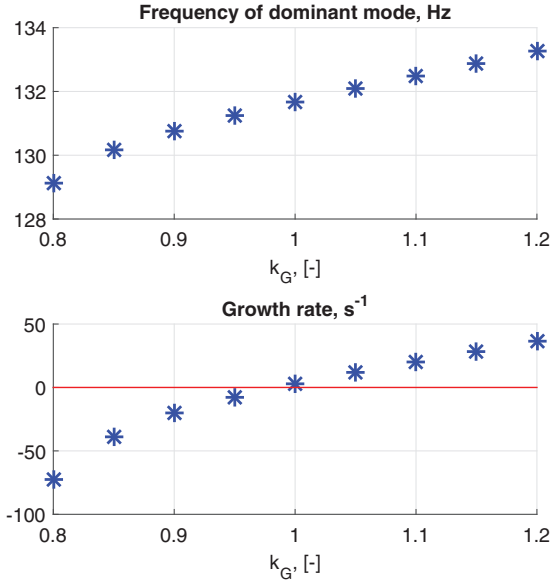
Figure 16. Dominant frequency of oscillations and its growth rate for various values of k_G parameter; $L_{c.c} = 0.7$ m, $x_{flame} = 0.03$ m, $\tau_{add} = 0$ ms.
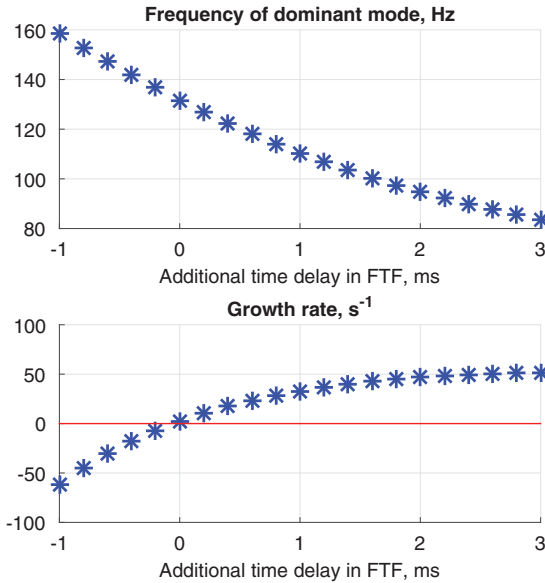

Figure 18. Dominant frequency of oscillations and its growth rate for various values of Δx_{flame} parameter; $L_{c.c} = 0.7$ m, $k_G = 1$, $\tau_{add} = \Delta x_{flame}/\bar{u}_r$.

Figure 17. Dominant frequency of oscillations and its growth rate for various values of τ_{add} parameter; $L_{c.c} = 0.7$ m, $x_{flame} = 0.03$ m, $k_G = 1$.

Sensitivity to the phase of FTF. Then, we vary the parameter τ_{add} in the range -1.0 to 3.0 ms with steps of 0.2 ms. The lower limit of this range is set by the value τ_f. The set-up is unstable for higher values of τ_{add}, i.e. higher absolute values of the phase of the FTF, as it can be seen from Figure 17. The dominant frequency of oscillations decays significantly when τ_{add} is increasing. The unstable frequency 100.3 Hz corresponds
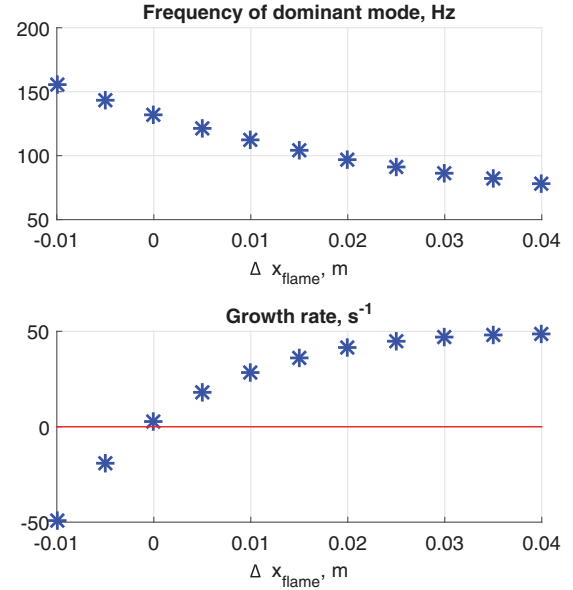
to $\tau_{add} = 1.6$ ms. Almost the same frequency 101.3 Hz was retrieved experimentally. It is because the phase of the FTF obtained numerically is underestimated with respect to the experimental one. Adding artificial time delay to the FTF obtained numerically shifts the phase of the FTF closer to the experimental one.

Combined sensitivity to the flame length and the FTF phase. Next, the influence of the simultaneous change of the flame position in the network model and the FTF phase on the stability is studied. The change of the FTF phase τ_{add} is assumed to be dependent on the change of the flame position in the network model Δx_{flame} as

$$\tau_{add} = \frac{\Delta x_{flame}}{\bar{u}_r} \tag{24}$$

where $\bar{u}_r = 11.3$ m/s. The length of the network model section *Combustor 1* is calculated as $x_{flame} = 0.03 + \Delta x_{flame}$. The dependence of the frequency of the dominant mode and its growth rate on both the flame location in the network model and the FTF phase are shown in Figure 18. $\Delta x_{flame} = 0.015$ m is characterised with the unstable frequency 104.1 Hz that is close to the frequency 101.3 Hz retrieved experimentally. Note that the resulting flame position $x_{flame} = 0.03 + 0.015 = 0.045$ m is almost the same as the heat release distribution maximum position in the experiment (see Figure 6).

The acoustic response of the flame with $\Delta x_{flame} = 0.015$ m is calculated by performing simulations in the network model considering only sections
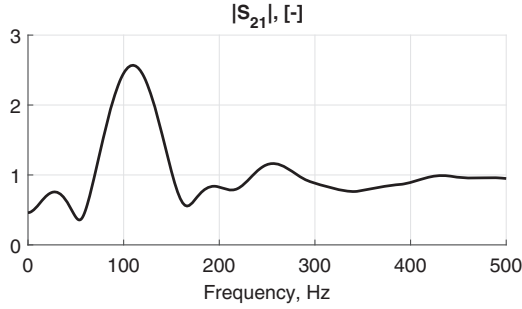
Figure 19. Acoustic response of the flame with $\Delta x_{flame} = 0.015$ m; $L_{c.c} = 0.7$ m, $k_G = 1$, $\tau_{add} = \Delta x_{flame}/\bar{u}_r$.
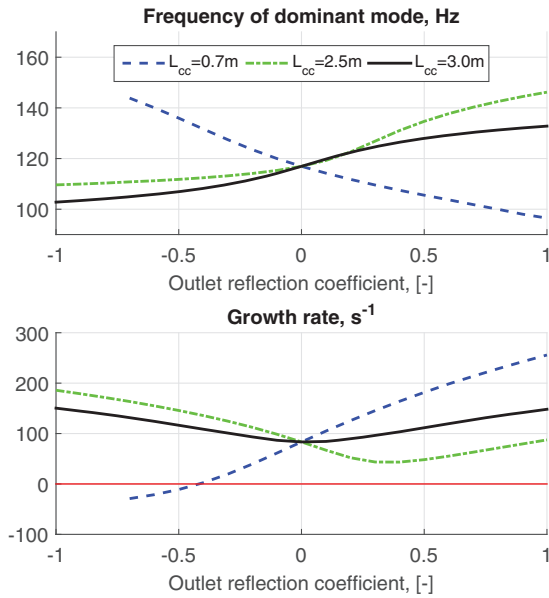

Figure 20. Dominant frequency of oscillations and its growth rate for various values of outlet reflection coefficient; $x_{flame} = 0.03$ m, $k_G = 1$, $\tau_{add} = 0$ ms.

Burner tube 3 and *Combustor 1*, as shown in Figure 12. The resulting $S_{21}(\omega)$ is shown in Figure 19. The maximum value of S_{21} with $\Delta x_{flame} = 0.015$ m corresponds to the frequency 109 Hz that is close to the unstable frequency revealed in the experiment.

Sensitivity to the outlet reflection coefficient. At the end, the influence of the outlet reflection on the stability of the system is studied. With the combustor length $L_{c.c} = 0.7$ m, the growth rate of the dominant mode increases while increasing the value of the reflection coefficient in the whole range $R_{out} = -0.7$ to 1, as shown in Figure 20. The frequency of the dominant mode decreases continuously while increasing the value of the reflection coefficient, in particular, when the reflection coefficient changes its sign. This behaviour

is different from the typical behaviour of acoustic mode. Moreover, the dominant mode remains unstable for the value of reflection coefficient $R_{out} = 0$, i.e. anechoic boundary condition. Silva et al.[27] have shown numerically that increasing the value of the outlet reflection coefficient makes the ITA mode more unstable. Note that the combustion chamber in the study of Silva et al.[27] was shorter than one-eighth of the acoustic wavelength of the ITA mode computed in their work.

For values of the outlet reflection coefficient in the range $R_{out} = -1$ to -0.8, unstable mode of 991 Hz that corresponds to the mode of the burner tube is computed. This frequency is beyond the frequency limit of the FTF computed in this work and it is not shown here.

The dependence of the ITA mode stability on the outlet reflection coefficient strongly depends on the length of the combustion chamber and how it correlates to the acoustic wavelength of the ITA mode computed with $R_{out} = 0$

$$\lambda_{ITA} = \frac{c_s}{f_{ITA}} = \frac{850}{118} = 7.2 \text{ m} \qquad (25)$$

If $L_{c.c} > \lambda_{ITA}/8$, another dependence of the ITA mode stability on R_{out} value is computed. For example, with $L_{c.c} = 3.0$ m the minimum growth rate is computed for $R_{out} = 0$. Meanwhile, with $L_{c.c} = 2.5$ m the reflection coefficient value $R_{out} = 0.4$ is characterised by the lowest growth rate value. Note that for any length of the combustion chamber with $R_{out} = 0$ unstable mode with the same frequency and growth rate is computed since no acoustic wave is travelling upstream from the outlet when $R_{out} = 0$.

5. Conclusions and future investigations

In this work, a two-step analysis of combustion instabilities in the time domain is proposed. The first step is to obtain the FTF of the system performing URANS simulations with the FSC model implemented in OpenFOAM. Since the FSC model has the improved treatment of the diffusion and the influence of the shear stress on the flame speed with respect to the more common TFC, the FSC model is preferable. The second step is to perform time-domain simulations using wave-based approach implemented in Simulink with the FTF obtained from the first step. Such simulations can predict the linear stability of the thermoacoustic system with the FTF and the weakly nonlinear analysis can be done once the FDF of the set-up is computed.

This two-step approach is applied to a laboratory test rig and it is shown that the proposed method is

able to predict combustion instabilities. The unstable mode computed in simulations corresponds to the unstable mode detected in experiments that is an ITA mode. Usage of the FSC model has improved the stability prediction with respect to the studies where the TFC model was used. The stability of the calculated mode depends significantly on the length of the combustion chamber, the gain and phase of the FTF and the outlet reflection coefficient; it depends less on the flame position. The frequency of this mode strongly depends on the phase of the FTF and the outlet reflection coefficient; its dependence on the length of combustor, the flame position and the gain of the FTF is less pronounced.

The next stage of the investigation is to compute the FDF of the set-up and to retrieve the appropriate model for the computed FDF. The flame model recently published by Tay-Wo-Chong et al.[30] that take into account heat losses can be used in future investigations of set-ups with heat losses.

Declaration of Conflicting Interests

The author(s) declared no potential conflicts of interest with respect to the research, authorship, and/or publication of this article.

References

1. Lieuwen TC and Yang V. Combustion instabilities in gas turbine engines: Operational experience, fundamental mechanisms, and modeling. *Progress in Astronautics and Aeronautics*. Reston, VA: American Institute of Aeronautics and Astronautics, 2005.
2. Huang Y and Yang V. Dynamics and stability of lean-premixed swirl-stabilized combustion. *Prog Energy Combus Sci* 2009; 35: 293–364.
3. Sirignano WA. Driving mechanisms for combustion instability. *Combust Sci Technol* 2015; 187: 162–205.
4. Nicoud F, Benoit L, Sensiau C, et al. Acoustic modes in combustors with complex impedances and multidimensional active flames. *AIAA J* 2007; 45: 426–441.
5. Camporeale S, Fortunato B and Campa G. A finite element method for three-dimensional analysis of thermoacoustic combustion instability. *J Eng Gas Turbines Power* 2011; 133: 011506.
6. Rofi L, Campa G, Anisimov V, et al. Numerical procedure for the investigation of combustion dynamics in industrial gas turbines: LES, RANS and thermoacoustics. In: *Proceedings of the ASME turbo expo 2015*, Montreal, Canada, paper no. GT2015-42168, 5–19 June 2015, p. V04AT04A016. DOI: 10.1115/GT2015-42168.
7. Pankiewitz C and Sattelmayer T. Time domain simulation of combustion instabilities in annular combustors. *J Eng Gas Turbines Power* 2003; 125: 677–685.
8. Li J and Morgans A. Time domain simulations of non-linear thermoacoustic behaviour in a simple combustor using a wave-based approach. *J Sound Vib* 2015; 346: 345–360.
9. Lipatnikov A and Chomiak J. Turbulent flame speed and thickness: phenomenology, evaluation, and application in multi-dimensional simulations. *Prog Energy Combus Sci* 2002; 28: 1–74.
10. *OpenFOAM version 2.3.0 User Guide*, 2014, http://cfd.direct/openfoam/user-guide/ (2014, accessed 5 February 2014).
11. Dowling A and Stow S. Acoustic analysis of gas turbine combustors. In: Lieuwen T and Yang V (eds) *Combustion instabilities in gas turbine engines*, chapter 13. Reston, VA: American Institute of Aeronautics and Astronautics, 2005, pp.369–414.
12. Bellucci V, Schuermans B, Nowak D, et al. Thermoacoustic modeling of a gas turbine combustor equipped with acoustic dampers. *J Eng Gas Turbines Power* 2005; 127: 372–379.
13. Bothien MR, Noiray N and Schuermans B. Analysis of azimuthal thermo-acoustic modes in annular gas turbine combustion chambers. *J Eng Gas Turbines Power* 2015; 137: 061505-1-8.
14. Komarek T and Polifke W. Impact of swirl fluctuations on the flame response of a perfectly premixed swirl burner. *J Eng Gas Turbines Power* 2010; 132: 061503.
15. Sayadi T, Le Chenadec V, Schmid PJ, et al. Thermoacoustic instability – a dynamical system and time domain analysis. *J Fluid Mech* 2014; 753: 448–471.
16. Dowling A. Nonlinear self-excited oscillations of a ducted flame. *J Fluid Mech* 1997; 346: 271–290.
17. Gentemann A, Yuen S and Polifke W. Influence of boundary reflection coefficient on the system identifiability of acoustic two-ports. In: *Proceedings of the 11th international Congress on sound and vibration*, Saint-Petersburg, Russia, 5–8 July 2004, pp.3501–3508. IIAV.
18. Luzzato C and Morgans A. The effect of a laminar moving flame front on thermoacoustic oscillations of an anchored ducted V-flame. *Combus Sci Technol* 2015; 187: 410–427.

19. Bothien M, Moeck J, Lacarelle A, et al. Time domain modelling and stability analysis of complex thermoacoustic systems. *Proc IMechE, Part A: J Power and Energy* 2007; 221: 657–668.

20. Iurashev D, Campa G, Anisimov V, et al. Turbulent flame models for prediction of pressure oscillations in gas turbine burners. In: *Proceedings of the 22nd international Congress on sound and vibration,*, Florence, Italy, 12–16 July 2015. IIAV.

21. Karpov V, Lipatnikov A and Zimont V. A model of premixed turbulent combustion and its validation. *Arch Combus* 1994; 14: 125–141.

22. Polifke W, Poncet A, Paschereit C, et al. Reconstruction of acoustic transfer matrices by instationary computational fluid dynamics. *J Sound Vib* 2001; 245: 483–510.

23. Tay-Wo-Chong L, Bomberg S, Ulhaq A, et al. Comparative validation study on identification of premixed flame transfer function. *J Eng Gas Turbines Power* 2012; 134: 021502–1,8.

24. Tay-Wo-Chong Hilares LR. *Numerical simulation of the dynamics of turbulent swirling flames.* PhD thesis, Technical University of Munich, Germany, 2012.

25. Poinsot T and Lele S. Boundary conditions for direct simulations of compressible viscous flows. *J Comput Phys* 1992; 101: 104–129.

26. Idelchik I. *Handbook of hydraulic resistance, 3rd Edition.* Moscow: Mashinostroenie, 1992.

27. Silva C, Emmert T, Jaensch S, et al. Numerical study on intrinsic thermoacoustic instability of a laminar premixed flame. *Combus Flame* 2015; 162: 3370–3378.

28. Tay-Wo-Chong L and Polifke W. Large eddy simulation-based study of the influence of thermal boundary condition and combustor confinement on premix flame transfer functions. *J Eng Gas Turbines Power* 2013; 135: 021502–1,9.

29. Bomberg S, Emmert T and Polifke W. Thermal versus acoustic response of velocity sensitive premixed flames. *Proc Combus Inst* 2015; 35: 3185–3192.

30. Tay-Wo-Chong L, Zellhuber M, Komarek T, et al. Combined influence of strain and heat loss on turbulent premixed flame stabilization. *Flow Turbul Combus* 2016; 97: 263–294.

Appendix I

Matrices for jump conditions between sections for the case of area decrease are

$$\mathbf{F}_{decr} = \begin{bmatrix} \dfrac{S_d}{\bar{c}_{s,d}}(1+M_d) & \dfrac{S_u}{\bar{c}_{s,u}}(1-M_u) \\ \dfrac{1}{\bar{\rho}_d}(1+M_d(1+\zeta_{decr})) & -\dfrac{1}{\bar{\rho}_u}(1-M_u) \end{bmatrix}$$

$$\mathbf{K}_{decr} = \begin{bmatrix} \dfrac{S_u}{\bar{c}_{s,u}}(1+M_u) & \dfrac{S_d}{\bar{c}_{s,d}}(1-M_d) \\ \dfrac{1}{\bar{\rho}_u}(1+M_u) & -\dfrac{1}{\bar{\rho}_d}(1-M_d(1+\zeta_{decr})) \end{bmatrix}$$

where S is the cross-section area, M is the mean Mach number and ζ is the coefficient of pressure losses.

Matrices for jump conditions between sections for the case of area increase are

$$\mathbf{F}_{incr} = \begin{bmatrix} \dfrac{S_d}{\bar{c}_{s,d}}(1+M_d) & \dfrac{S_u}{\bar{c}_{s,u}}(1-M_u) \\ \dfrac{1}{\bar{\rho}_d}(1+M_d) & -\dfrac{1}{\bar{\rho}_u}(1-M_u(1-\zeta_{incr})) \end{bmatrix}$$

$$\mathbf{K}_{incr} = \begin{bmatrix} \dfrac{S_u}{\bar{c}_{s,u}}(1+M_u) & \dfrac{S_d}{\bar{c}_{s,d}}(1-M_d) \\ \dfrac{1}{\bar{\rho}_u}(1+M_u(1-\zeta_{incr})) & -\dfrac{1}{\bar{\rho}_d}(1-M_d) \end{bmatrix}$$

Matrices for jump conditions between sections for the case of temperature jump with active flame and constant cross-section area are

$$\mathbf{J} = \begin{bmatrix} (1+2M_d+M_d^2) & -(1-2M_u+M_u^2) \\ \left[\dfrac{\bar{c}_s+\gamma\bar{u}}{\gamma-1}+\dfrac{3\bar{u}^2}{2\bar{c}_s}+\dfrac{\bar{u}^3}{2\bar{c}_s^2}\right]_d & -\left[\dfrac{\bar{c}_s-\gamma\bar{u}}{\gamma-1}+\dfrac{3\bar{u}^2}{2\bar{c}_s}-\dfrac{\bar{u}^3}{2\bar{c}_s^2}\right]_u \end{bmatrix}$$

$$\mathbf{H} = \begin{bmatrix} (1+2M_u+M_u^2) & -(1-2M_d+M_d^2) & 0 \\ \left[\dfrac{\bar{c}_s+\gamma\bar{u}}{\gamma-1}+\dfrac{3\bar{u}^2}{2\bar{c}_s}+\dfrac{\bar{u}^3}{2\bar{c}_s^2}\right]_u & -\left[\dfrac{\bar{c}_s-\gamma\bar{u}}{\gamma-1}+\dfrac{3\bar{u}^2}{2\bar{c}_s}-\dfrac{\bar{u}^3}{2\bar{c}_s^2}\right]_d & \dfrac{1}{s} \end{bmatrix}$$

where γ is the heat capacity ratio.